IEEE Access
Multidisciplinary | Rapid Review | Open Access Journal

Received 16 August 2023, accepted 4 September 2023, date of publication 13 September 2023,
date of current version 21 September 2023.

Digital Object Identifier 10.1109/ACCESS.2023.3314796

RESEARCH ARTICLE

Motility Analysis of Diaphragm in Patients With Chronic Pulmonary Lung Disease Based on Computed Tomography Technique

HAO YU[1], NNUBIA PASCAL NNAMDI[1], ARIA SEO[1], JINKYEONG PARK[2], AND YUNSIK SON[1]

[1]Department of Computer Science and Engineering, Dongguk University, Jung-gu, Seoul 04620, South Korea
[2]Department of Pulmonary, Allergy and Critical Care Medicine, Kyung Hee University College of Medicine, Kyung Hee University Hospital at Gangdong, Gangdong-gu, Seoul 05278, South Korea

Corresponding authors: Jinkyeong Park (pjk3318@gmail.com) and Yunsik Son (sonbug@dongguk.edu)

This work was supported in part by the National Research Foundation of Korea (NRF) under Grant NRF-2020R1C1C1009091 and Grant 2018R1A5A7023490, in part by the Ministry of Science and ICT (MSIT) of the Government of the Republic of Korea, and in part by the MSIT of the Government of the Republic of Korea through the Information Technology Research Center (ITRC) Program Supervised by the Institute for Information and Communication Technology Planning and Evaluation (IITP) under Grant IITP-2023-2020-0-01789.

This work involved human subjects or animals in its research. Approval of all ethical and experimental procedures and protocols was granted by the Institutional Review Board (IRB) under Approval Nos. DUIH2020-04-012 and KHNMC 2022-03-063-008.

ABSTRACT The diaphragm plays a crucial role in respiration, and diaphragm dysfunction is common in COPD, contributing to worsening symptoms and higher mortality rates. Many methods have been implemented to evaluate the function of the diaphragm, but each comes with its unique set of limitations. To overcome this challenge, a novel approach was introduced to assess diaphragm function in patients with chronic obstructive pulmonary disease (COPD) using thoracic computed tomography scans. This novel approach involves generating a simulation of the diaphragm from lung DICOM slice images and calculating the dynamic change in respiratory motion by quantifying the difference in the simulated diaphragm mesh area during inhalation and exhalation. The experimental design incorporates various image processing algorithms, computational geometry algorithms, and a surface fitting algorithm optimized to minimize the potential sources of error. When the proposed technique was applied to detect diaphragmatic dysfunction in patients with COPD, the results of the Pearson correlation analysis showed a strong relationship between the variables ratio of exhalation to inhalation surface and average z-value difference inhalation and exhalation surfaces, with a coefficient of 0.731. The results suggest that the proposed technique is highly accurate and beneficial in scenarios where diaphragm function is essential, such as respiratory disorders, neuromuscular diseases like Amyotrophic Lateral Sclerosis or muscular dystrophy, spinal cord injuries, and conditions such as sleep apnea. By providing specific numerical data on sensitivity and specificity, this approach offers a quantitative evaluation of its effectiveness in detecting diaphragmatic dysfunction in patients with COPD. In conclusion, the proposed approach is currently semi-automated, however, future study may investigate fully automated approaches using this technique.

INDEX TERMS Chronic obstructive pulmonary disease, computed tomography, diaphragm segmentation, digital image processing, medical image computing.

I. INTRODUCTION

The diaphragm plays a vital role in the process of respiration. As the diaphragm contracts and flattens during inhalation, it increases the volume of the thoracic cavity and decreases the pressure within it, allowing air to flow into the lungs. Conversely, during exhalation, the diaphragm relaxes and resumes its dome shape, reducing the volume of the thoracic cavity and increasing the pressure, which forces air out of the lungs. In chronic obstructive pulmonary disease

The associate editor coordinating the review of this manuscript and approving it for publication was Hengyong Yu.

(COPD), characterized by limited airflow in the airways, the diaphragm's role becomes even more critical. COPD patients often experience shortness of breath and difficulty exhaling due to narrowed airways.

Diaphragm dysfunction is observed not only in severe COPD cases but also across all stages of the disease. Diaphragm dysfunction often presents as unilateral paralysis, which can be challenging to detect. However, when patients lie down or engage in excessive movement, they may experience significant breathing difficulties due to this dysfunction [1]. Diaphragm dysfunction can contribute to worsening COPD patients' conditions [2]. It can lead to an increased hospitalization rate due to exacerbations, and consequently, it can also contribute to a higher mortality rate among COPD patients [3].

Diaphragm function has been assessed using various methods, which include evaluating the position and shape of the diaphragm on chest X-rays, measuring muscle electrical activity through electromyography (EMG), observing diaphragm movement during respiration using fluoroscopy, and employing non-invasive techniques, such as ultrasound, to examine diaphragm thickness and movement [4], [5], [6], [7]. However, such methods have limitations, including difficulties in assessing the entire diaphragm, variability between evaluators, and challenges in quantifying the results objectively. Recently, some studies have introduced MRI for evaluating diaphragm function [8]. Still, due to lung lesions, the use of MRI is rare and can be challenging to incorporate into routine patient care for assessing the diaphragm. Generally, in COPD patients, the diaphragm muscle's length, shortness, and mobility decrease as a compensatory mechanism due to hyperinflation. Based on the hypothesis that the difference in the diaphragm's area during inhalation and exhalation on COPD inspiratory CT scans will be significantly reduced, we aim to explore a method to assess the diaphragm's movement and shape using thoracic CT scans, which are commonly used in the diagnosis and treatment of airway diseases. The contribution of this paper is to provide a new technique that examines the impact of chronic obstructive pulmonary disease (COPD) on the thoracic diaphragm. It focuses on the simulation of the diaphragm from the CT Lung slices before calculating the dynamic change in respiratory motion by quantifying the difference in the simulated diaphragm. First, to simulate the movement of the diaphragm, CT lung slices are taken as input data. Afterward, various computational methods were used, including image processing algorithms, computational geometry algorithms, and a surface fitting algorithm to segment the diaphragm region. The segmented diaphragm is then analyzed to gain insights into the dynamics of respiratory motion and better understand how the diaphragm contributes to breathing. The analysis validates the methodology used as it shows that when the diaphragm moves more during breathing, it also extends more during exhalation and becomes larger in size. This knowledge may be beneficial for creating respiratory system models that are more accurate, for enhancing medical imaging and diagnosis, and perhaps even for developing new respiratory ailment treatments.

A. PREPARATION AND PROCESSING OF CHEST COMPUTED TOMOGRAPHY (CT) IMAGES

1) STUDY POPULATION

The Medical Research Ethics Review Committee of Dongguk University Ilsan Hospital (DUIH2020-04-012) and Kyung Hee University Hospital (KHNMC2022-03-063-008) at Gangdong approved this retrospective study. In addition, it should be noted that some patients from the group of 70 smokers without pulmonary function impairments and the group of 94 smokers with airway obstruction were not included in the analysis due to the unavailability of appropriate scanned images. Therefore, the final sample size for this retrospective study was 100 lower than the initially collected 164 patient CT scanned Digital Imaging and Communications in Medicine (DICOM) images. The study was conducted with the approval of the Medical Research Ethics Review Committee of Dongguk University Ilsan Hospital (DUIH2020-04-012) and Kyung Hee University Hospital (KHNMC2022-03-063-008) at Gangdong.

2) IMAGE ACQUISITION - CT PROTOCOL

Inspiratory CT scans were obtained at the end of full inspiration, and expiratory CT scans were obtained at the end of forced expiration. All CT scans were obtained using 16-multidetector CT scanner (Somatom Sensation; Siemens Medical Systems, Erlangen, Germany). Scan parameters included 16 $\times$ 0.75 mm collimation, 100 effective mAs, 140 kVp, and pitch 1.0. Both scans were performed in a supine position. All CT scans were performed without contrast medium. The images were reconstructed using standard soft tissue kernel (B30f; Siemens Medical Systems) with 0.75 mm of thickness and 0.7 mm of increment.

B. IMAGE PROCESSING USING OPENCV

OpenCV is a widely used, cross-platform open-source library with programming functions. It is implemented in C, C++, and Python, making it compatible with various operating systems, including Linux, Windows, and macOS. This robust library is extensively employed in image-processing applications across multiple fields, including engineering, security, and medicine. By utilizing image processing techniques like RGB-to-grayscale conversion, erosion, and dilation, OpenCV provides a reliable and efficient means of manipulating digital images.

Furthermore, OpenCV's versatility extends beyond its core functionality. In image processing, numerous innovative applications have emerged that leverage OpenCV's capabilities. These applications address crucial challenges in domains such as digital crime evidence management [9], personal portfolio authentication [10], and weakness static analysis [11]. By incorporating cutting-edge technologies

TABLE 1. Bitwise operations for various image processing needs.

Operator	Usage	Description
Bitwise AND	a AND b	Returns true if and only if both pixels are greater than zero.
Bitwise OR	a OR b	Returns true if either of the two pixels is greater than zero.
Bitwise XOR	a XOR b	Returns true if and only if one of the two pixels is greater than zero, but not both.
Bitwise NOT	NOT a	Inverts the "on" and "off" pixels in an image.

like blockchain, Hyperledger Fabric, and Bidirectional Encoder Representations from Transformers (BERT) models, these advancements push the boundaries of what is possible in their respective fields. OpenCV's robustness and flexibility make it a fundamental tool for implementing these image-processing techniques and achieving significant progress in image manipulation tasks.

1) MORPHOLOGICAL TRANSFORMATION

Morphological transformations are a set of operations that process images based on their shapes. It is usually performed on binary images and is used to reduce image features. They apply structuring elements or kernels to the input images and produce output images. Erosion and dilation are two fundamental morphological operators used to analyze and restore structures in an image. Erosion operations suppress features on a surface. In contrast to erosion, dilation operations increase the number of features present on a surface by adding pixels to region boundaries [12].

2) SUZUKI'S CONTOUR ALGORITHM

Suzuki's border-following algorithm retrieves contours from the binary images. Suzuki's algorithm is based on the hierarchical relationship between border pixels obtained from an image. The algorithm first scans the image to extract border pixels that belong to the boundary. Then criteria are set to determine whether it is an outer or a hole border. Finally, execution terminates when the criteria are satisfied [13].

3) OPEN CV BITWISE OPERATIONS

Bitwise operations such as AND, OR, NOT, and XOR are commonly used in the field of computer vision. These operations are applied to grayscale images where each pixel is represented by a numeric value between 0 and 255. A pixel value of 0 is considered ''off,'' while a value greater than 0 is considered ''on,'' analogous to the concepts of false and true in Boolean algebra. These operations are commonly used in image processing, as listed in Table 1 [14].

C. 3D POINT CLOUD-RELATED ALGORITHMS

A 3D point cloud is considered a simple and powerful representation of static and dynamic 3D objects in various research areas, ranging from object recognition to reconstruction. Compared to 3D meshes, 3D point clouds have better performance and lower overhead due to their simple and flexible representation. Despite these advantages, point clouds contain a large amount of data that is subject to outliers and noise. Therefore, to obtain accurate 3D point clouds, it is essential to perform additional outlier filtering and simplification operations.

1) OUTLIER REMOVAL

Outliers, also referred to as noise data, are data points that exhibit characteristics that are significantly different from the majority of data points within the same class. The presence of outliers can negatively affect the validity and reliability of datasets. Common causes of outliers include incorrect inputs, measurement error, data manipulation, mislabeling, and sampling error. Several outlier-detection techniques have been developed to identify and handle outliers. These can be broadly classified into three categories: decision-boundary-based, cluster-based, and statistics-based techniques. Decision-boundary-based techniques randomly partition the data to identify isolated points. In cluster-based techniques, outliers are identified based on their distance from the cluster centroid. Statistics-based techniques identify points that are farther from their neighbors than the mean distance.

2) POINT CLOUD SIMPLIFICATION

Point clouds are collections of data points in three-dimensional coordinate systems that can contain a large number of individual points. Simplification techniques may be used to reduce the number of points in a point cloud, while preserving the essential features of the original model. Examples of such techniques include hierarchical clustering simplification (HCS) and Gaussian sphere simplification (GS), which are implemented using the computational geometry algorithm library (CGAL) and MATLAB, respectively. Another method for point cloud simplification is the curvature-based 2-point importance method (CV) method, which is implemented using Open3D [15].

D. MESH-RELATED ALGORITHMS

1) ALPHA COMPLEX

Alpha complex is a well-known algorithm used for converting a 3D point cloud into a polygon mesh. It is based on Delaunay triangulation of a given set of points, and forms a structure of nonoverlapping triangles connecting the points. Although the alpha complex has important applications in computational geometry, it has been found to have non-monotonic properties that can render it useless in certain contexts. Despite this limitation, the alpha complex remains a useful tool for estimating the shape and form of three-dimensional objects from point-cloud data [16].

2) THE QUICKHULL ALGORITHM FOR CONVEX HULLS

A convex hull of a geometric shape is defined as the minimum convex quantity that encloses it. This concept can be formally defined as the intersection of all convex sets that contain a given subset of Euclidean space or, alternatively, as the set of all convex combinations of points within the subset. When considering bounded subsets of planes, the convex hull can be thought of as a shape enclosed by a rubber band stretched around the subset. Quickhull is an algorithm for computing the convex hull of a finite set of points in an n-dimensional space, using a divide-and-conquer approach similar to quicksorting [17].

3) BALL-PIVOTING ALGORITHM FOR SURFACE RECONSTRUCTION

The ball-pivoting algorithm constructs triangular meshes from point clouds using a region-growing interpolation technique. This algorithm is known for its ability to produce accurate mesh results and is implemented in the MeshLab software. The algorithm works by placing a constructed ball on the surface of the point cloud creating a seed triangle based on the points where the ball touches the surface. The ball was then moved to the edge of this triangle using the intersection of two points, and a triangle was added to the mesh by merging the two vertices. In this way, the ball-pivoting algorithm iteratively grows a triangular mesh from the point cloud data [18].

4) INTERSECTION OF D-DIMENSIONAL ISO-ORIENTED BOX

A hyperrectangle, also called a D-dimensional iso-oriented box, is a rectangular box that exists in d-dimensional space, where d is the number of intervals in the Cartesian product. The function CGAL::Polygon_mesh_processing::do_intersect [19], [20] is a useful tool for detecting intersections between a large number of hyperrectangles, also known as bounding boxes, which are simplified versions of complex geometric shapes. The do_intersect function can be used to detect intersections and self-intersections of polyhedral surfaces. These are 3D shapes composed of multiple faces, edges, and vertices, using the bounding boxes of triangles in space as input. This allows efficient determination of intersection points between these triangles.

5) AREA MEASUREMENT OF TRIANGULATED SURFACE MESH

The ball-pivoting algorithm produces triangular meshes that allow the calculation of the total area of the mesh by summing the areas of all the triangles that make it up. However, if the shape of the mesh is complex or irregular, the variational shape approximation (VSA) method can be used to approximate the input surface mesh by a simpler triangular mesh. This method is based on approximating a surface with a set of triangular facets, which allows for a more concise representation of the shape, while maintaining some degree of accuracy. The VSA method has gained acceptance in various fields due to its efficiency and effectiveness in approximating surfaces [21].

E. MULTITHREADING AND CONCURRENCY IN C++

Performing computationally intensive geometric operations such as the intersection of d-dimensional iso-oriented boxes, can be a time-consuming process. To solve this problem, the use of multithreading and concurrency techniques in C++ can reduce execution time. The execution thread refers to a discrete sequence of program instructions that can be managed independently by the scheduler. Simultaneous execution of multiple threads within a single process can be achieved through multithreading, which enables the sharing of resources, such as memory, among threads. In contrast, individual processes do not share resources. It is worth noting that threads within a process also share access to the process's executable code and the values of its dynamically allocated variables and nonthread-local global variables [22].

F. SURFACE FITTING USING MATLAB GRIDFIT

GRIDFIT [23] is an algorithmic approach used for generating smooth surfaces from point clouds in three-dimensional space. It is particularly effective in situations where the data are scattered or semi-scattered, as it is able to effectively interpolate and smooth any irregularities in the data. The algorithm divides the point cloud into a mesh of cells and then uses various interpolation techniques to estimate the values of the points within those cells. The most commonly used interpolation methods include bilinear, nearest-neighbor, and linear interpolation. Bilinear interpolation involves continuous estimation of data within a grid, whereas nearest-neighbor interpolation estimates multidimensional data by identifying the points closest to the target location and using their values. On the other hand, linear interpolation involves the linear estimation of data within triangular cells created by dividing the mesh. GRIDFIT has numerous practical applications, including scientific visualization, computer graphics, and data analysis.

II. PROPOSED METHODOLOGY

Based on the constraints discussed in the previous section, we present a semi-automatic algorithm for simulating the diaphragm. The experimental plan is shown in Figure 1 and includes the following nine steps, which are explained in detail in the following subsections.

1. Obtain CT data and extract the corresponding image and metadata.
2. Identify the coordinates of all points within the Hounsfield unit range of the lungs [−700, −600 [24]] using the linear transformation formula for pixels and HU values.
3. Remove all abnormal points under and around the lungs.

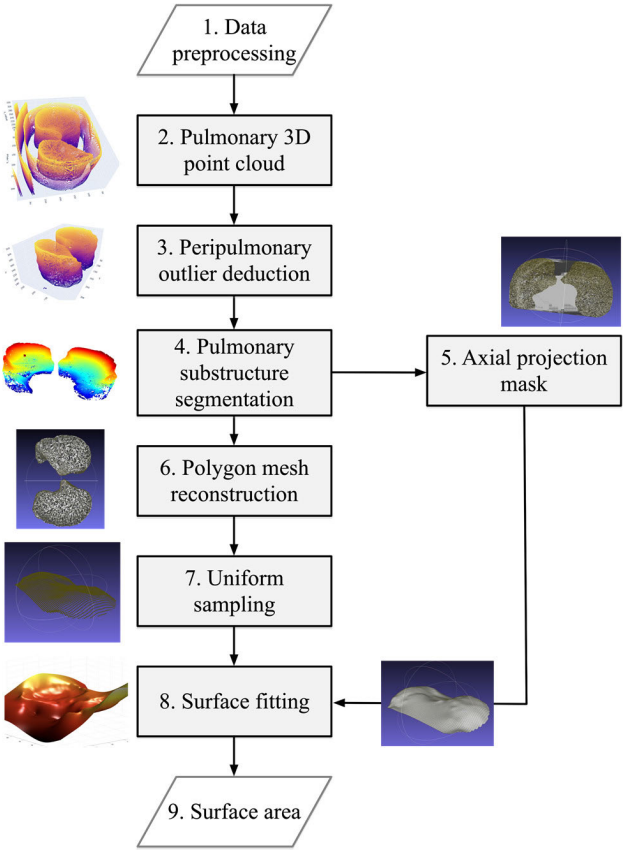

FIGURE 1. Flowchart of the experimental design.

4. Segment the point cloud at the bottom of the lungs and convert it to a mesh using the Alpha Complex algorithm.
5. Create an axial projection of the point cloud at the bottom of the lungs and obtain its boundary points as a surface mask.
6. Use collision-based uniform sampling to obtain points on the virtual surface.
7. Use GRIDFIT (from MATLAB) for surface fitting, and then apply the previously generated surface mask to segment the pulmonary-diaphragmatic contact surface.
8. Calculate the area of the mesh using the CGAL (Computational Geometry Algorithms CGAL::Polygon _mesh_processing::area function, and apply a correction for Library's area using formula for the lateral area of frustums.
9. Compute the ratio of inspiratory and expiratory areas to diagnose and evaluate the diaphragm.

A. EXPERIMENTAL THREE-DIMENSIONAL CARTESIAN COORDINATE SYSTEM REPRESENTATION

The x-, y-, and z-axes used in the present study correspond to the anteroposterior, horizontal, and cephalocaudal anatomical axes, respectively, as shown in Figure 2. These axes are oriented anterior to posterior, right to the left, and superior to inferior. The range of values for these axes is determined by the number of pixel rows and columns, usually 512, and the thickness of the slice to be analyzed.

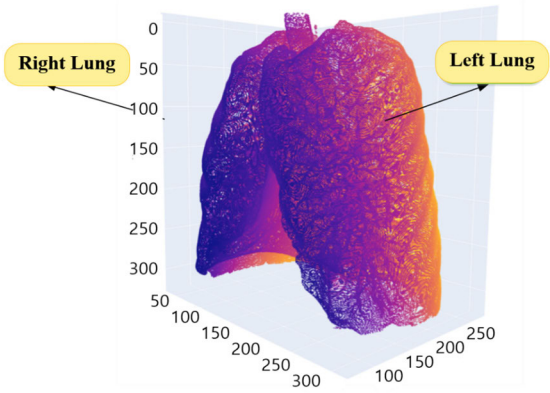

FIGURE 2. A 3D point cloud of a patient's inhalation visualized with Plotly [25].

B. DATA PREPROCESSING

First, the original data containing a set of images is imported using the Horos® medical image viewer which provides image processing features. Next, to ensure the CT images were arranged in the correct anatomical order, rather than relying solely on the lexicographic ordering of the DCM image file name as shown in Figure 5, the metadata information was reviewed to confirm the position and orientation of each image. It is worth noting that file names alone may not always provide reliable information on the order of medical images. Therefore, we verified the sequence of images based on their anatomical structures to ensure accurate analysis. Subsequently, the CT images were verified, and the required subset images were exported for further.

C. ACQUISITION OF PULMONARY THREE-DIMENSIONAL POINT CLOUD

Convert the raw values of pixel intensities to Hounsfield units (HU) using the linear transformation of (1) [26].

$$I_{HU} = I_o \cdot s + i \tag{1}$$

In the given equation (1), I_{HU} represents the pixel intensity value in HU, I_o refers to the raw intensity value obtained from the CT scanner before conversion to HU, and s and i are the rescale slope and intercept, respectively. The linear transformation conducted in (1) is a crucial for converting raw pixel intensities to Hounsfield Units, to ensure meaningful representation of tissue densities in CT images. It involves calibrating the pixel intensities in the CT images and mapping them to generate meaningful tissue densities. The rescale slope and intercept parameters in the equation are determined during the CT scanner calibration process to adjust and scale the raw pixel intensities to the appropriate HU values. Figure 3 shows the visualization results after the linear transformation.

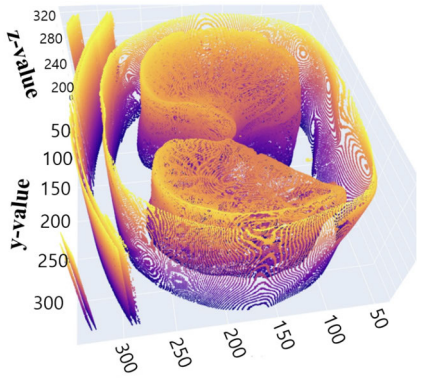

FIGURE 3. Schematic diagram of the point cloud at the bottom of the lung located in the HU interval of the lung ([−700, −600]).

D. PERIPULMONARY OUTLIER DEDUCTION

Figure 6 shows redundant noise data present at the base and near the lung, which can be eliminated using the algorithm in Figure 4. The algorithm involves thorax denoising, morphological transformations, binary thresholding, contour tracing, and bitwise operations to extract the lung region from a CT scan. However, using the Hounsfield unit (HU) range of [−700, −600] to extract the lower region of the lung, it shows the possibility of extracting other organs at the lower end of the lungs. Therefore, a manual noise eliminating approach was implemented using the MeshLab 3D mesh processing software to remove noise data at the base of the lungs.

E. PULMONARY SUBSTRUCTURE SEGMENTATION AND POLYGON MESH RECONSTRUCTION

As shown in Figure 5, the denoised 2D lung images were transformed into a 3D point cloud by integrating slice thickness metadata. The pulmonary substructure is identified by traversing all *y0z* planes and by selecting the point with the highest z value that intersects the line y = N (where N is in the range [0, 300]) in each plane. For the extraction of the pulmonary substructure, the x0y plane with the greatest number of points was determined as the contact surface and taken as the center, with an extension of 40 mm in the upward and downward directions. Finally, the Alpha complex algorithm is applied to transform the 3D point cloud into a mesh.

F. UNIFORM SAMPLING OF BASED ON COLLISION DETECTION

The determination of the coordinates of the contact surface can be achieved be creating several polylines and then intersecting them with the mesh located at the base of the lungs, as shown in Figure 6. When an intersection point is observed, the corresponding coordinate points are recorded.

G. SURFACE FITTING OF THE PULMONARY-DIAPHRAGMATIC CONTACT SURFACE

The 3D contact surface can be fitted with MATLAB's GRIDFIT function with planar contact points that are generated by applying the collision-detection algorithm, as shown in Figure 7.

The pulmonary substructure mask was extracted using a method similar to the collision algorithm, as shown in Figure 8. The 3D point cloud of the pulmonary substructure was first squashed along the z-axis, and then the convex hull algorithm was applied to the resulting mesh to create the mask mesh. The surface was then reconstructed using the alpha shape algorithm, and the boundary points of the convex hull mesh were obtained from the *l2r* and *r2l* directions. The surface mesh was obtained by applying the ball pivoting surface reconstruction algorithm to the 3D point cloud of the surface inside the mask, as shown in Figure 9.

H. PROPERTIES AND AREA CORRECTION FOR SURFACE MESHES

In Figure 10, it is shown that when the position of the simulated diaphragm at the base of the lung is conceptualized as a plane, the part of the diaphragm between the exhalation and inhalation positions is not be taken into account. Therefore, the lateral area of the frustum, as shown in Figure 11 and described in (2), is used to simulate this excluded part of the diaphragm.

$$A_{Lateral} = \pi R_2 \sqrt{H^2 + (R_2 - R_1)^2} \tag{2}$$

The area of the simulated diaphragm can be obtained using the mesh area calculation algorithm described above. If it is approximated as two circles, then R_1 and R_2 can be obtained using the circle area formula. The average height difference H can be obtained by uniform sampling from the two meshes of exhalation and inhalation. Therefore, the corrected area corresponding to the overlying exhalation portion, can be determined using (2).

III. EXPERIMENTAL RESULTS

A. EXPERIMENTAL ENVIRONMENT

In this study, graphics-related operations were performed on a high-performance server using concurrent processing time optimization techniques. The experimental environment is presented in Table 2 and Table 3. Other tasks, including experimental process control and manual mesh processing, were performed on a MacBook. On average, the test took approximately 17 min on a single patient.

B. RESULTS AND EVALUATION

In this study, the experiment was conducted on a cohort of 82 patients, with each patient having over 500 DICOM image scans. The patients were stratified into two categories consisting of 41 patients with COPD and 41 patients without COPD (i.e., "NORMAL" patients). The sample size for this study initially included 164 patients. However, due to the unavailability of Pulmonary Function Tests (PFTs) for some of the patients, the final sample size was reduced to 82 patients. As a result, a subset of randomly selected patients, consisting of

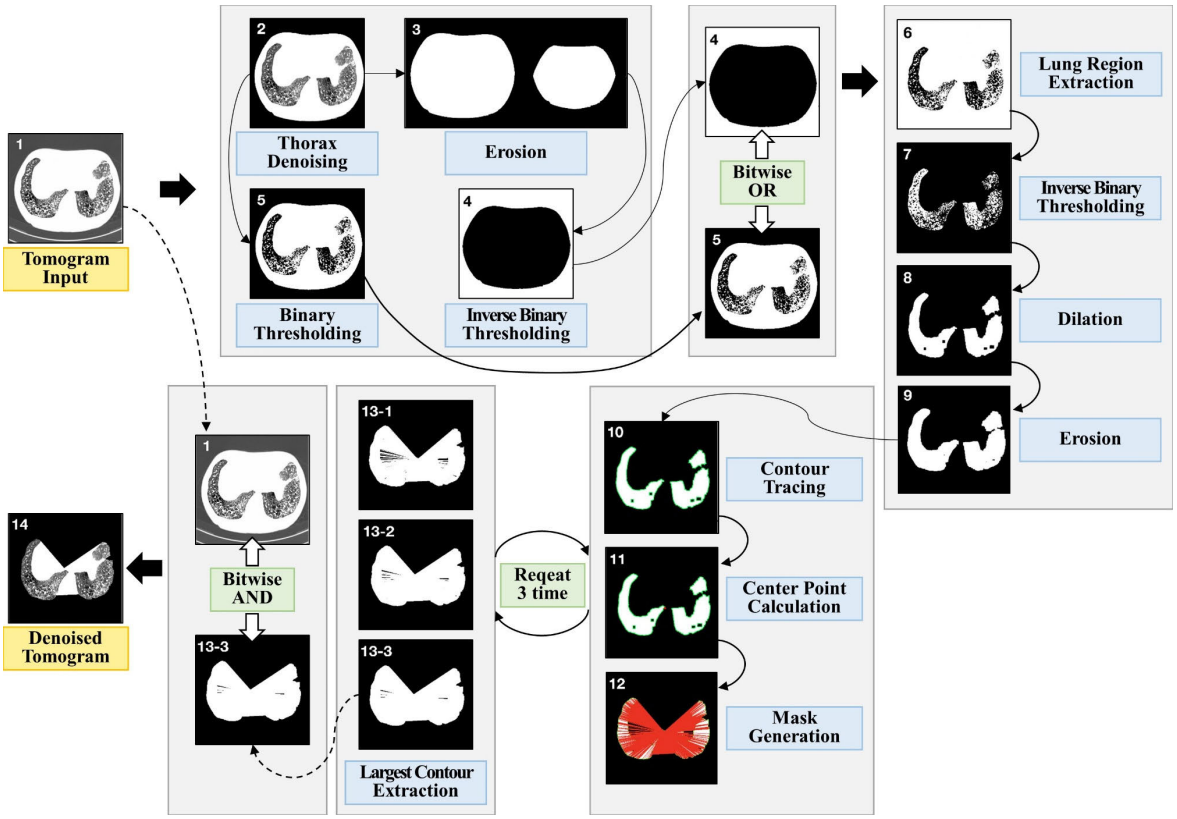

FIGURE 4. Peripulmonary outlier deduction algorithm.

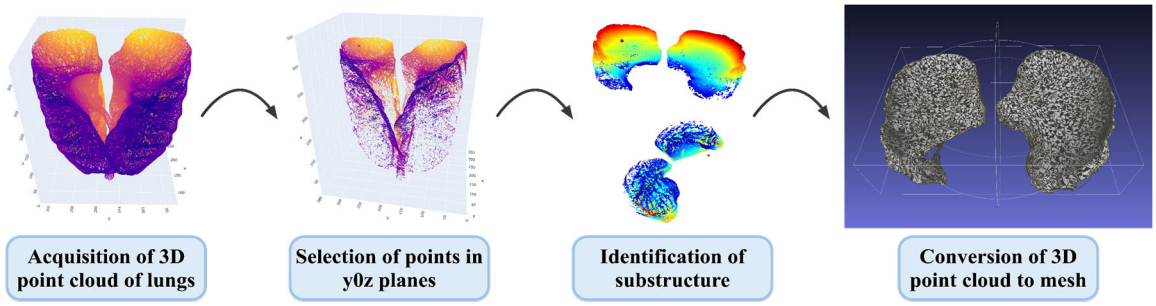

FIGURE 5. Pulmonary substructure segmentation and polygon mesh reconstruction algorithm.

41 patients with COPD and 41 patients without COPD (i.e., "NORMAL" patients), was used for the analysis. Figure 12 displays a graph with data from 20 patients, representing 10 patients with COPD and 10 patients without COPD, which is a representative subset of the entire cohort. The aim of this experiment was to examine potential distinctions between these two patient groups based on their respective DICOM image datasets. To maintain patient confidentiality and protect their privacy, the patient IDs were anonymized to ensure the original patients IDs are not exposed while preserving its data information for analysis. The average height difference between the inhalation and exhalation surfaces is represented by the variable labeled "avg. z-val diff in. & exh. surfaces" in Figure12. The "ratio of exhalation to inhalation surface" variable in Figure 12 on the other hand measures the proportion of the exhalation surface area to the inhalation surface area. These two metrics provide important insights into the relationship between the morphology of the inhalation and exhalation surfaces and the development of COPD.

Figure 12 indicates that individuals with chronic obstructive pulmonary disease (COPD) have a significantly higher ratio of exhalation to inhalation surface (A) and a higher average z-value differential in the exhalation and inhalation surfaces (B) as compared to those without the condition. This demonstrates a strong correlation between the two variables and attests to the reliability of the approach proposed in the study. Overall, the information in Figure 13 provides significant insights into the relationship between COPD and

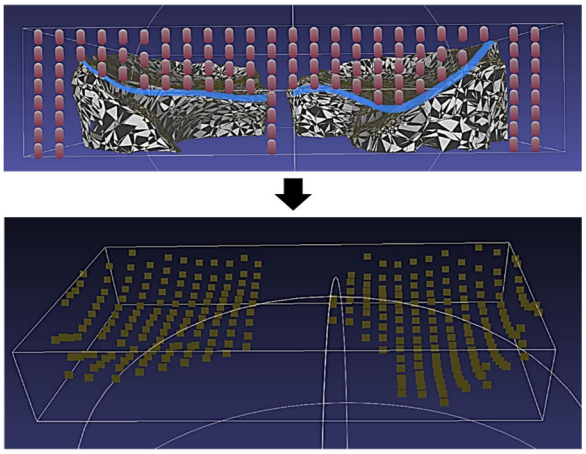

FIGURE 6. Schematic diagram of the collision detection algorithm.

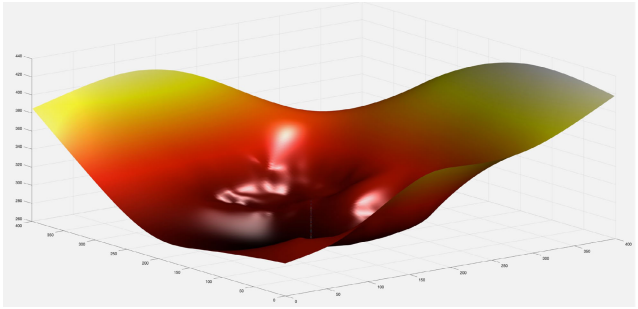

FIGURE 7. Pulmonary-diaphragmatic contact surface fit using GRIDFIT with collision detection points.

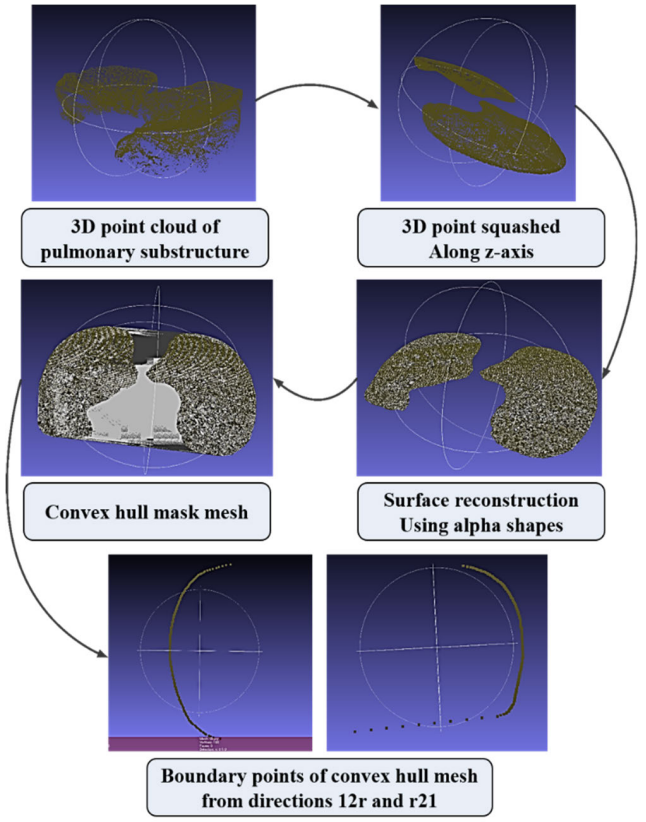

FIGURE 8. Generating mask for pulmonary substructure.

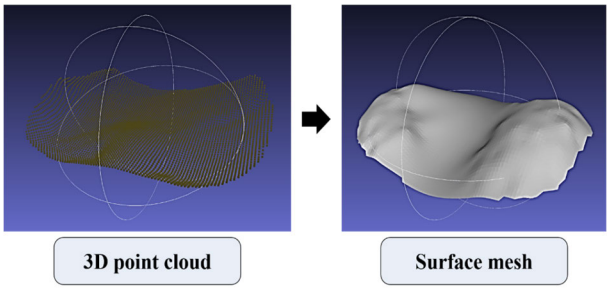

FIGURE 9. Obtaining the surface mesh using the ball pivoting algorithm on the 3D point cloud.

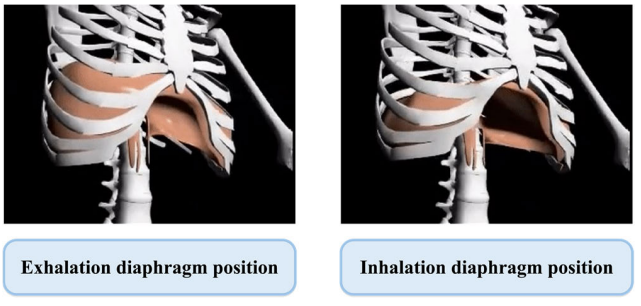

FIGURE 10. Diagram of the position of the diaphragm during exhalation and inhalation.

various metrics related to inhalation and exhalation surfaces, emphasizing the potential significance of these variables in understanding the development and progression of the disease. It also suggests that the development of COPD may be a result of an increase in the diaphragm's upward and downward movement during respiration.

"z-value_difference" represents the difference between expiratory and inspiratory surfaces. These differences tend to decrease as mobility decreases. For patients with COPD in our data who had significantly reduced FEV1 (mean $\pm$ SD; 1.84 ± 0.68) compared to patients without COPD (3.30 ± 0.58, $P < 0.001$), the Z-values show significantly more minor differences than those without COPD (32.81 ± 19.28 vs. 45.90 ± 18.62, $p = 0.002$).

A statistically significant correlation was found between the difference in diaphragm cross-sectional area during inhalation and exhalation and the decrease in expiratory volume per second (FEV1) as airway obstruction increased Figure 14 (A). This correlation was even more pronounced when the subgroup of individuals with COPD was considered in Figure 14 (B).

The results of the Pearson correlation analysis, show a strong relationship between the variables ratio of exhalation to inhalation surface and avg. z-val diff in. & exh. surfaces, with a coefficient of 0.731. This relationship is further supported by a significance level of zero, which is below the threshold of 0.05, indicating a statistically significant

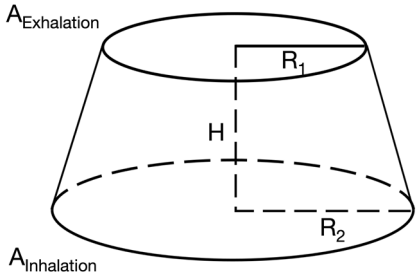

FIGURE 11. Schematic diagram of the area correction.

TABLE 2. Linux experimental environment for computationally intensive geometric intersection operations.

Software development tools	CLion 2022.1.2
	GNU Compiler Collection 11.3.0
	CMake 3.23.2
	Boost 1.79.0
	CGAL 5.4.2

TABLE 3. macOS experimental environm ent for experimental process control.

Hardware specifications	CPU	Apple M1 Pro (8) @ 3.22 GHz
	RAM	32 Gigabytes
System software	OS	macOS 12.2.1 (Build 21D62)
Software development tools	PyCharm 2021.3.2 (Professional Edition)	
	MeshLab v2022.02[27]	
	IBM SPSS Statistics 26	
	MATLAB R2021a	
	Python 3.10.4	
	Pydicom 2.3.0	
	OpenCV 4.5.5	
	Pandas 1.4.2	
	Pyntcloud 0.2.0	
	CGAL 5.4.2	

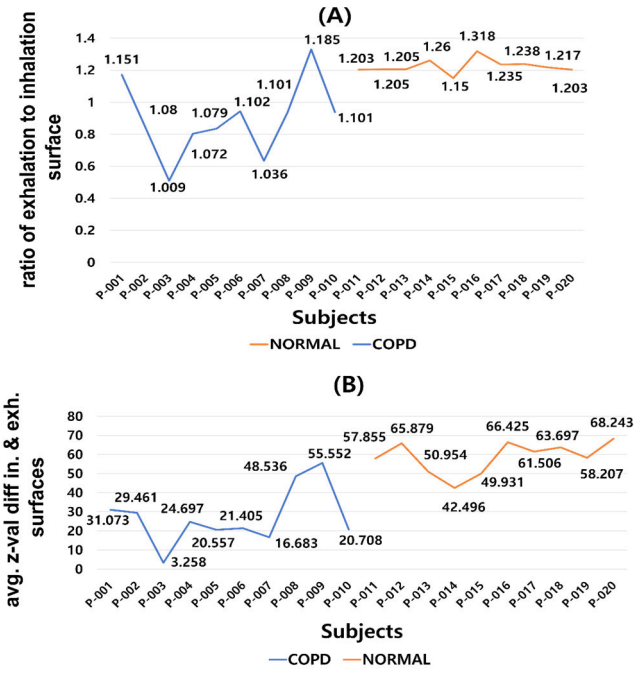

FIGURE 12. Comparison of the ratio of exhalation to inhalation surface(A) and the average z-value differential in the exhalation and inhalation surfaces(B) in patients with and without COPD.

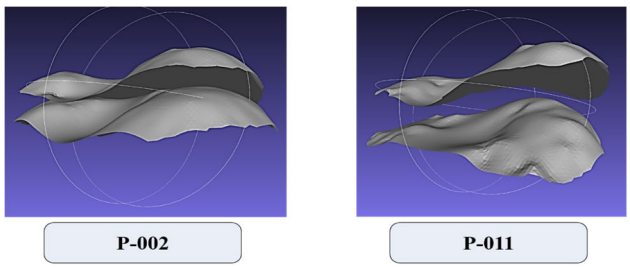

FIGURE 13. Diaphragm mobility during respiration based on area ratio or height difference.

relationship. From this, it can be concluded that there is a significant connection between the two variables. Correlation analysis validates the methodology used as it supports the contention that an increase in the upward and downward movement of the diaphragm during respiration results in a corresponding increase in the extension of the diaphragm during exhalation and a larger diaphragm area ratio.

IV. DISCUSSION AND LIMITATIONS

This study introduced a novel approach for objective and quantitative evaluation of diaphragm function. Our approach presented a semi-automatic method that created a diaphragm simulation from lung CT images. By evaluating the difference in the simulated diaphragm mesh area during inhalation and exhalation, we could calculate the dynamic changes in respiratory motion. The proposed method allows for an additional evaluation of diaphragm function using only existing CT, offering an objective way to understand a patient's condition changes and helping to predict their prognosis without requiring additional radiation exposure or exam.

Our semi-automatic approach offers multiple advantages. This method can be employed using actual lung CT images that are typically acquired in clinical practice which does not call for any additional hardware or equipment. Our method is not computationally complex compared to other techniques that require sophisticated equipment or demanding procedures. In addition, our approach can be used to assess differences in diaphragm function over time, which is particularly helpful for individuals with chronic respiratory conditions or undergoing medical interventions that may affect diaphragm function. Additionally, the proposed method is more objective than ultrasound-based measurements, as results can be checked by anyone, rather than solely the person performing the measurement.

The well-established understanding that persistent airflow limitation can result in hyperinflation, thereby diminishing

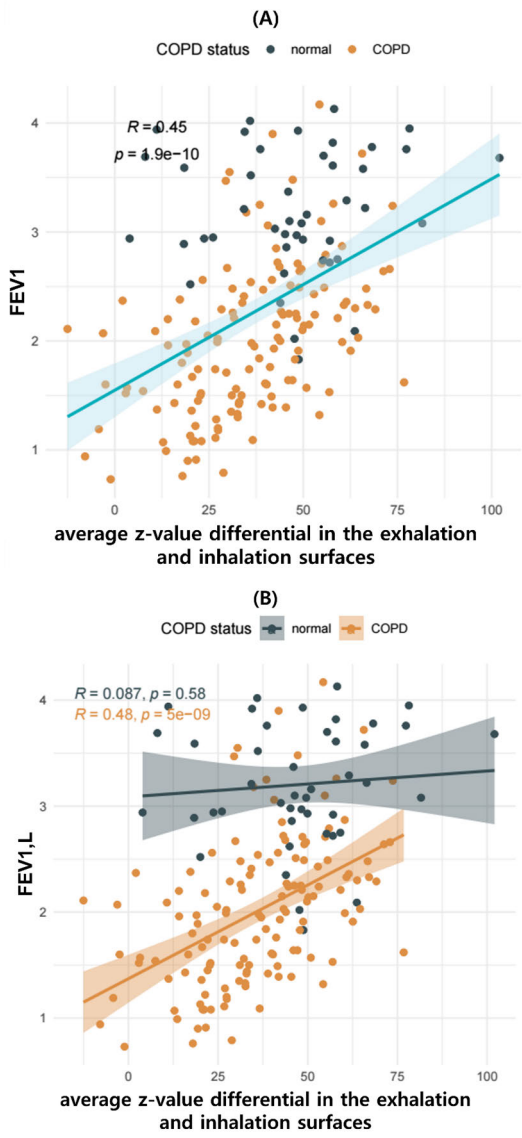

FIGURE 14. A statistically significant correlation was found between the difference in diaphragm cross-sectional area during inhalation and exhalation and the decrease in expiratory volume per second (FEV1) increased. This correlation was even more pronounced in the subgroup of individuals with COPD.

diaphragm movement, is a significant concern. This progression often escalates dyspnea symptoms, undermines pulmonary function, and leads to a poorer clinical prognosis. It is hypothesized that an increase in the severity of airflow limitation could correspond to a reduced range of diaphragmatic motion during respiration. This hypothesis has been substantiated by our study, which identified a statistically significant correlation between the degree of diaphragmatic surface area change during respiration, as determined by our novel methodology, and Forced Expiratory Volume in one second (FEV1), a key indicator representing the extent of airflow limitation. However, as the methodology used in this study is unique, direct comparison to existing techniques might be challenging. More research is needed to compare this method directly with others to demonstrate its advantages and possible limitations.

Even though our method appears promising for assessing diaphragm function, it's necessary to note that our study has significant drawbacks. First, our sample size may have limited how far we could generalize our results. As our study was limited to patients with a specific respiratory ailment, it is also essential to assess the applicability of our approach in patient groups with different diseases such as neuromuscular disease or paralysis of the diaphragm, or spinal cord injury. Second, the study provides a snapshot of the relationship between diaphragm function and FEV1 at a given point in time. Longitudinal studies could provide insights into how this relationship evolves, particularly in response to treatments or disease progression. Third, while the proposed method shows promise, further studies are needed to determine how it can be best implemented in a clinical setting. This includes understanding its cost-effectiveness, the time required for analysis, and the training required for medical professionals to use the method. Fourth, As the methodology used in this study is unique, direct comparison to existing tools might be challenging. More research is needed to compare this method directly with others to demonstrate its advantages and possible limitations. Although there are limitations to our proposed method of diaphragm segmentation, our semi-automatic method for evaluating diaphragm function is a useful and practical approach that is simple to apply in clinical practice. Further studies are required to confirm our approach in larger patient datasets and to evaluate its applicability in other therapeutic settings.

V. CONCLUSION

This study presents a novel approach for assessing diaphragmatic function using thoracic computed tomography scans, offering a temporal evaluation that could help determine the risk of exacerbation or predict prognosis in patients with chronic airway diseases. The approach proposed in this study could be beneficial for assessing diaphragmatic function in various conditions and therapeutic settings. However, further research is necessary to validate and refine this method and confirm its applicability and effectiveness with larger patient datasets. This methodology could guide the provision of personalized care for these patients.

AUTHOR'S CONTRIBUTIONS

Conceptualization: Jinkyeong Park; methodology: Hao Yu, Nnubia Pascal Nnamdi, Jinkyeong Park, and Yunsik Son; software: Hao Yu, Nnubia Pascal Nnamdi, and Yunsik Son; formal analysis: Jinkyeong Park and Aria Seo; data curation: Jinkyeong Park, Hao Yu, and Nnubia Pascal Nnamdi; writing-original draft preparation: Hao Yu, Nnubia Pascal Nnamdi, and Aria Seo; writing-review and editing: Jinkyeong Park, Aria Seo, and Yunsik Son; visualization: Hao Yu, Nnubia Pascal Nnamdi, and Yunsik Son; supervision: Jinkyeong Park and Yunsik Son; project administration: Jinkyeong Park and

Yunsik Son; and funding acquisition: Jinkyeong Park and Yunsik Son. All authors have read and approved the final manuscript.

ACKNOWLEDGMENT

The current study was conducted after obtaining approval from the Institutional Review Board (IRB) under protocol numbers DUIH2020-04-012 and KHNMC 2022-03-063-008, and all participants provided written informed consent.

REFERENCES

[1] J. C. Hogg and W. Timens, "The pathology of chronic obstructive pulmonary disease," *Annu. Rev. Pathol., Mech. Disease*, vol. 4, no. 1, pp. 435–459, Feb. 2009, doi: 10.1146/annurev.pathol.4.110807.092145.

[2] B. Bordoni and Zanier, "Anatomic connections of the diaphragm influence of respiration on the body system," *J. Multidisciplinary Healthcare*, vol. 6, p. 281, Jul. 2013, doi: 10.2147/JMDH.S45443.

[3] D. Testelmans, T. Crul, K. Maes, A. Agten, M. Crombach, M. Decramer, and G. Gayan-Ramirez, "Atrophy and hypertrophy signalling in the diaphragm of patients with COPD," *Eur. Respiratory J.*, vol. 35, no. 3, pp. 549–556, Mar. 2010, doi: 10.1183/09031936.00091108.

[4] N. Hindley, P. Keall, J. Booth, and C. Shieh, "Real-time direct diaphragm tracking using kV imaging on a standard linear accelerator," *Med. Phys.*, vol. 46, no. 10, pp. 4481–4489, Oct. 2019, doi: 10.1002/MP.13738.

[5] E. Karami, Y. Wang, S. Gaede, T.-Y. Lee, and A. Samani, "Anatomy-based algorithm for automatic segmentation of human diaphragm in noncontrast computed tomography images," *J. Med. Imag.*, vol. 3, no. 4, Nov. 2016, Art. no. 046004, doi: 10.1117/1.JMI.3.4.046004.

[6] *Anatomical Terms of Location—Wikipedia*. Accessed: Nov. 25, 2022. [Online]. Available: https://en.wikipedia.org/wiki/Anatomical_terms_of_location

[7] W. D. Bidgood, S. C. Horii, F. W. Prior, and D. E. Van Syckle, "Understanding and using DICOM, the data interchange standard for biomedical imaging," *J. Amer. Med. Inform. Assoc.*, vol. 4, no. 3, pp. 199–212, May 1997, doi: 10.1136/jamia.1997.0040199.

[8] T. D. DenOtter and J. Schubert, "Hounsfield unit," Radiopaedia.org, StatPearls Publishing, Treasure Island, FL, USA, Tech. Rep., Mar. 2022, doi: 10.53347/rid-38181.

[9] D. Kim, S.-Y. Ihm, and Y. Son, "Two-level blockchain system for digital crime evidence management," *Sensors*, vol. 21, no. 9, p. 3051, Apr. 2021.

[10] J. Jeong, D. Kim, S.-Y. Ihm, Y. Lee, and Y. Son, "Multilateral personal portfolio authentication system based on hyperledger fabric," *ACM Trans. Internet Technol.*, vol. 21, no. 1, pp. 1–17, Feb. 2021.

[11] D. H. Nguyen, A. Seo, N. P. Nnamdi, and Y. Son, "False alarm reduction method for weakness static analysis using BERT model," *Appl. Sci.*, vol. 13, no. 6, p. 3502, Mar. 2023.

[12] N. Jamil, T. M. T. Sembok, and Z. A. Bakar, "Noise removal and enhancement of binary images using morphological operations," in *Proc. Int. Symp. Inf. Technol. (ITSim)*, vol. 3, Aug. 2008, pp. 1–6, doi: 10.1109/ITSIM.2008.4631954.

[13] S. Suzuki and K. Be, "Topological structural analysis of digitized binary images by border following," *Comput. Vis., Graph., Image Process.*, vol. 30, no. 1, pp. 32–46, Apr. 1985, doi: 10.1016/0734-189X(85)90016-7.

[14] S. Ansari, "Techniques of image processing," in *Building Computer Vision Applications Using Artificial Neural Networks*. Berkeley, CA, USA: Apress, 2020, pp. 27–94, doi: 10.1007/978-1-4842-5887-3_3.

[15] S. Wang, Q. Hu, D. Xiao, L. He, R. Liu, B. Xiang, and Q. Kong, "A new point cloud simplification method with feature and integrity preservation by partition strategy," *Measurement*, vol. 197, Jun. 2022, Art. no. 111173, doi: 10.1016/j.measurement.2022.111173.

[16] H. Edelsbrunner and E. P. Mücke, "Three-dimensional alpha shapes," *ACM Trans. Graph.*, vol. 13, no. 1, pp. 43–72, Jan. 1994, doi: 10.1145/174462.156635.

[17] C. B. Barber, D. P. Dobkin, and H. Huhdanpaa, "The quickhull algorithm for convex hulls," *ACM Trans. Math. Softw.*, vol. 22, no. 4, pp. 469–483, Dec. 1996, doi: 10.1145/235815.235821.

[18] F. Bernardini, J. Mittleman, H. Rushmeier, C. Silva, and G. Taubin, "The ball-pivoting algorithm for surface reconstruction," *IEEE Trans. Vis. Comput. Graphics*, vol. 5, no. 4, pp. 349–359, Dec. 1999, doi: 10.1109/2945.817351.

[19] S. Loriot, M. R. Labbé, J. Tournois, and I. O. Yaz, "Polygon mesh processing," in *CGAL User and Reference Manual*, 5.6 ed. CGAL Editorial Board, 2023. [Online]. Available: https://doc.cgal.org/5.5/Manual/packages.html#PkgPolygonMeshProcessing

[20] A. Zomorodian and H. Edelsbrunner, "Fast software for box intersections," 2000, pp. 129–138, Accessed: Oct. 7, 2022. [Online]. Available: https://dl.acm.org/doi/pdf/10.1145/336154.336192

[21] D. Cohen-Steiner, P. Alliez, and M. Desbrun, "Variational shape approximation," in *Proc. ACM SIGGRAPH Papers*, Aug. 2004, pp. 905–194, doi: 10.1145/1186562.1015817.

[22] A. Williams and P. Multithreading, *C++ Concurrency in Action*. Shelter Island, NY, USA, 2019. Accessed: Oct. 11, 2022. [Online]. Available: https://www.manning.com/books/c-plus-plus-concurrency-in-action-second-edition

[23] J. D'Errico, "Surface fitting using gridfit," MATLAB Central File Exchange, Natick, MA, USA, 2022. Accessed: Jul. 30, 2022. [Online]. Available: https://www.mathworks.com/matlabcentral/fileexchange/8998-surface-fitting-using-gridfit

[24] E. Kazerooni and B. Gross. (2004). *Cardiopulmonary Imaging*. Accessed: Sep. 21, 2022. [Online]. Available: https://books.google.com/books?hl=en&lr=&id=IJwZHPrDQYUC&oi=fnd&pg=PP13&dq=Page+379+in:+Ella+A.+Kazerooni%3B+Barry+H.+Gross+(2004).+Cardiopulmonary+Imaging.+Vol.+4.+Lippincott+Williams+%26+Wilkins&ots=PS046Qz9oQ&sig=mQyewr9Yj6O9hzIKLbkUTIhyimA

[25] *Collaborative Data Science*, Plotly Technol., Montreal, QC, Canada, 2015. [Online]. Available: https://plot.ly

[26] N. Singh, S. Sonkesriya, S. B. Bagewadi, S. Anwar, S. Abraham, A. S. Parihar, and A. Mohammed, "Clinical assessment of bone quality at implant site using CBCT and Hounsfield unit," *J. Pharmacy Bioallied Sci.*, vol. 15, no. 2, pp. S1305–S1307, 2023.

[27] P. Cignoni, M. Callieri, M. Corsini, M. Dellepiane, F. Ganovelli, and G. Ranzuglia. *MeshLab: An Open-Source Mesh Processing Tool*. Accessed: Oct. 21, 2022. [Online]. Available: http://diglib.eg.org/bitstream/handle/10.2312/LocalChapterEvents.ItalChap.ItalianChapConf2008.129-136/129-136.pdf

HAO YU received the B.S.E. degree in computer science and engineering from Sogang University, Seoul, South Korea, in 2021, and the M.Eng. degree in computer engineering from Dongguk University, Seoul, in 2023. His current research interests include medical image analysis, software engineering, and deep learning.

NNUBIA PASCAL NNAMDI received the B.S.E. degree in computer science and engineering from the Department of Computer Science and Engineering, Dongguk University, Seoul, South Korea, in 2022, where he is currently pursuing the master's degree in computer science and engineering with the Department of Computer Science and Engineering. His research interests include secure software, medical image analysis, object detection and capturing, and software engineering.

ARIA SEO received the B.S. degree in management, and the M.S. and Ph.D. degrees in information technology from Dongguk University, Gyeongju-si, South Korea, in 2011, 2014, and 2018, respectively. She is currently a Research Professor with the Department of Computer Science and Engineering, Dongguk University, Seoul. Her research interests include cyber physical systems, smart media systems, smart polishing systems, and IT convergence software.

JINKYEONG PARK received the Medical degree from Ewha womans University, and the Ph.D. degree. She completed a residency in internal medicine with the Ewha Womans University Medical Center, followed by a fellowship in pulmonary disease and critical care medicine with the Asan Medical Center. She is currently a Physician with Kyung Hee University Hospital, Gangdong, Seoul, South Korea. She is board certified in critical care medicine, internal medicine, and pulmonary disease. Her clinical interests include chronic obstructive pulmonary disease (COPD) and emphysema, focusing on genetics in susceptibility to cigarette smoking. She also investigates artificial intelligence (AI) in respiratory and critical care medicine.

YUNSIK SON received the B.S., M.S., and Ph.D. degrees from the Department of Computer Science and Engineering, Dongguk University, Seoul, South Korea, in 2004, 2006, and 2009, respectively. He was a Research Professor with the Department of Brain and Cognitive Engineering, Korea University, Seoul, from 2015 to 2016. Currently, he is an Associate Professor with the Department of Computer Science and Engineering, Dongguk University. His research interests include secure software, programming languages, compiler construction, and mobile/embedded systems.